DAMAGE STATE ASSESSMENT OF FIBER REINFORCED METAL LAMINATE COMPOSITES

R. Carmi[1], B. Wisner[2], P.A. Vanniamparambil[3], R. Shneck[4], A. Bussiba[5] and A. Kontsos[6*]

[1]NRCN, Materials Department, Beer-Sheva, P.O.B 9001. Israel
Email: carmo_nm@netvision.net.il
[2]Theoretical & Applied Mechanics Group, Dept. of Mechanical Engineering and Mechanics, Drexel University, Philadelphia, PA 19104. USA
Email: bjwisner@gmail.com
[3]Theoretical & Applied Mechanics Group, Dept. of Mechanical Engineering and Mechanics, Drexel University, Philadelphia, PA 19104. USA
Email: prashanth288@gmail.com
[4]Department of materials engineering, Faculty of Engineering Sciences, Ben-Gurion University of the Negev, Beer-Sheva, P.O.B 653, 8499000. Israel.
Email: roni@bgumail.bgu.ac.il
[5]NRCN, Materials Department, Beer-Sheva, P.O.B 9001. Israel
Email: busarie@bezeqint.net
[6]Theoretical & Applied Mechanics Group Director, Department of Mechanical Engineering and Mechanics, Drexel University, Philadelphia, PA 19104, USA
*Corresponding Author: Email: antonios.kontsos@drexel.edu , Tel: +1 215 895 2297

Keywords: FRML, Glare, Mechanical properties, Acoustic Emission

Abstract
Fiber Reinforced Metal Laminate (FRML) composites are widely used as a structural material, mainly in the aerospace industry. One of the main challenges using FRML composites is to detect and asses/quantify damage during in-service conditions. For these reasons, the research presented in this article targets the development of a nondestructive testing and evaluation (NDT&E) method capable to assess damage development in FMRL composites as a function of applied loading. Specifically, the current research presents an approach based on multiscale observations which aims to monitor major failure modes in Glare®1A FRML specimens subjected to quasi-static loading conditions. Specifically, a combination of NDT&E methods is used including the Acoustic Emission (AE) and Digital Image Correlation (DIC) which are coupled with *in situ* Scanning Electron Microscope (SEM) level tensile tests. The post-processing of the ensemble of recorded AE activity reveals characteristics that were associated with the composite's constituents (Al-alloy as well as glass fibers within an epoxy matrix) along with features that were associated with delaminations and fiber/matrix interface failure. Furthermore, pronounced AE activity was detected at the elastic to plastic transition region which was found to evolve in a way similar to micro-crack density trends suggested by micro-mechanical models. The similarity noticed, motivated the use of specific AE features to evaluate the damage state evolution in FRML composites.

1. Introduction

Fiber Reinforced Metal Laminate (FRML) composites are widely used as a structural material in the aerospace industry. Among them Glare® possesses good overall mechanical and fatigue properties due to its structure which consists of fiberglass/epoxy layers between Al alloy sheets [1, 2]. Glare has been found to enable stress transfer to its metal layers when cracks are created, which reduces stress localizations; this process is referred to as "bridging effect" [3, 4]. For these reasons, Glare® is currently used in aerospace applications in critical load bearing components that need to withstand demanding loading conditions, such as the ones appearing in the cargo door of C-17 military transport aircraft or at the fuselage material in Airbus A380 [5]. The failure process in FRML composites such as Glare® is complex and involves multiple damage modes such as fiber fracture, matrix cracking, fiber-matrix debonding, interfacial shear failure, and delamination. When loaded in tension, fiber pull-out and shear failure modes are also observed, while in transverse tension matrix failure and matrix-fiber interface debonding are dominant.

In this article, the AE method is used as part of the experimental nondestructive testing and evaluation (NDT&E) approach. AE refers to the release of energy due to a sudden change in a material subjected to external loading [6, 7]. This phenomenon can be traced from the macro level at which cracks are visible e.g. at the structural scale to microscopic levels at which e.g. crystallographic effects in metals can be related to damage [6]. Irreversible processes related to damage are associated with the energy release in the form of elastic waves, which propagate throughout the bulk of the material and are eventually recorded by sensors. Each recorded AE signal can be parametrized by a number of time, frequency and energy features. In addition to signal processing, classification algorithms [6, 8] are used to group AE activity based on a number of selected features to associate such information with e.g. damage in the case of this article [9, 10].

In addition to AE, the DIC method is used to assess damage in Glare. This method provides full field deformation maps obtained while performing mechanical testing. DIC is capable of making such measurements using a set of images taken before and during a test [11]. Applying a random speckle pattern on the surface of the sample enables the system to measure surface deformation by tracking and correlating changes in the associated light intensity fields [11, 12], resulting in deformation measurements with ~50 micro strain (με) accuracy [13-16]. Using DIC as a complementary NDT&E method to AE has been shown by the authors to enable better understanding of the mechanical behavior across materials and scales [17, 18].

Damage modeling in FRML involves mathematical and numerical formulations that involve the activation and evolution of damage modes. An early model [19] assumed that the FRML is composed of several plies. In an unconstrained unidirectional ply, such as a ply that is not bonded to any others, a uniform tensile stress normal to the fiber orientation will cause failure at the fiber/matrix interface. Since the ply in reality is constrained within a laminate, actual failure does not result from a single delamination, instead, several interfacial cracks form as the stress increases [20-33]. Such sequence of events in the fracture process will be described and discussed in this article. The current research suggests a new approach in monitoring the damage evolution in Glare. This approach is explained in this article and is related on-going investigations related to damage assessment methods for this material.

2. Experimental procedures

The current research focuses on Glare®1A which consists of three layers of Aluminum 7475 T76 (0.3 mm in thickness each) as well as two layers of unidirectional S2 fiberglass (10 μm diameter) embedded in epoxy resin (FM94 with 0.25 mm thickness), as shown in (Figure 1a-b) [34]. In order to obtain a better understanding of the failure mechanisms, first the constituents materials, namely the alloy, the fibers and the epoxy resin were investigated in terms of mechanical and acoustical responses combined with

DIC measurements. Then, an experimental study performed on Glare®1A flat dog-bone specimens (6 mm in width and gauge length of 40 mm) including both mechanical and acoustical responses characterization was performed. The correlation between constituent and full specimen results was then used to infer on the capabilities of the described approach to assess the damage state in this material.

Tension tests were conducted using a servo-hydraulic machine using friction grips in displacement control at a crosshead velocity of 0.5mm/min. AE activity was tracked using a commercially MISTRAS Micro II AE system. Two resonant sensors (pico) connected to preamplifiers with set at 40 dB and a band-pass filter between 20 kHz-1MHz were used. A threshold of 30 dbae was selected with Peak Definition Time, Hit Definition Time and Hit Lockout Time of 100, 400 and 400 μsec respectively. DIC measurements were obtained by applying a random speckle pattern (black dots on white paint) on the specimen's surface for strain measurement using a 5 megapixel GOM 3D DIC system (Figure 1c). The system was calibrated for a field of view (FOV) of 55x44 mm; the cameras were positioned 40 cm away from the specimen which resulted in a strain sensitivity of 50 με with an imaging recording rate of 1 Hz. Metallographic and fractographic studies were performed in order to correlate the deformation features and fracture modes with the AE findings. Furthermore, *in situ* SEM tensile tests were also conducted combined with AE tracking in order to cross-validate the AE results with microstructure. The SEM level experiments were conducted with a tensile fixture composed of a screw-driven Gatan MTEST stage with a 2000 N load cell which was located at a FEI XL30 SEM chamber (Figure 1d). A constant displacement rate of 0.5 mm/min was used in these tests.

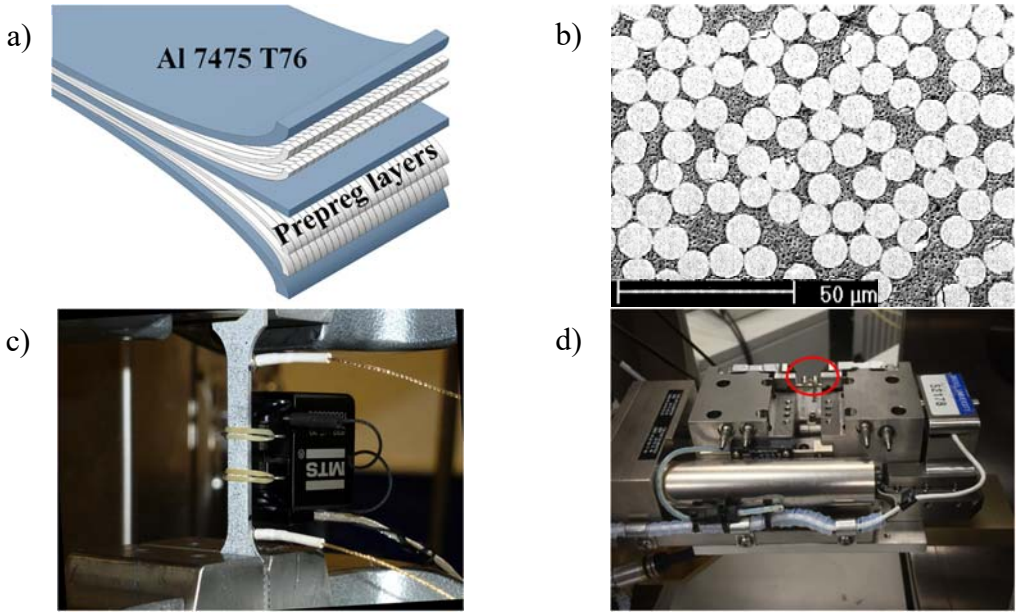

Figure 1. a) FRML Glare®1A structure [33], b) typical SEM image of prepreg layer (top view), c) Lab scale tensile test of Glare®1A dog-bone shape containing DIC spackle pattern, d) in-situ SEM tensile stage containing Glare®1A sample and 2 AE sensors (circled)

3. Experimental results

3.1. Glare®1A constituents

An investigation was first performed on Glare®1A constituents (Al-7475 T76, Prepreg, S2 fibers glass and epoxy resin FM94) and selected results are presented in Figure 2. Specifically, Figure 2a-b illustrates the stress-strain curve of Al 7475-T761 together with AE data in terms of AE counts and cumulative counts. In order to distinguish between the different deformation and failure mechanisms involved

during the fracture process, two types of classification algorithms were used [8]; the k-means and a neural network named Learning Vector Quantization (LVQ). The results revealed two main groups of AE signals that can be correlated to plastic deformation with peak frequency (PF) around 150 kHz and micro-cracking around 400 kHz (Figure 2b). Advanced classification methodologies, based on a weighted peak frequency (WPF) approach (reported in [35]) enable further assessment of such post-processing results as displayed in Figure 2b. Partial Power (PP) feature quantifies the percentage of power of a signal within a frequency range; in the current study PP3 was selected in order to evaluate the signal contribution between the range of 300-450 kHz. When combining the WPF data with the PP3 feature a clear distinction can be observed [36] as expressed in Figure 2b.These results are consistent with the DIC and microscopy findings in which deformation via macroscopic slip lines and microcracking of second-phase particles were observed. Furthermore, testing of S2 glass fiber bundles in Figure 2c shows a PF value of 450 kHz. Finally, Figure 2d illustrates the stress-strain curve of a single prepreg layer which resulted in a PF of 100 kHz attributed to matrix cracking, while other damage mechanisms such as interface matrix/fiber cracking emerges at 150 kHz and fibers breakage emerged again near 450 kHz.

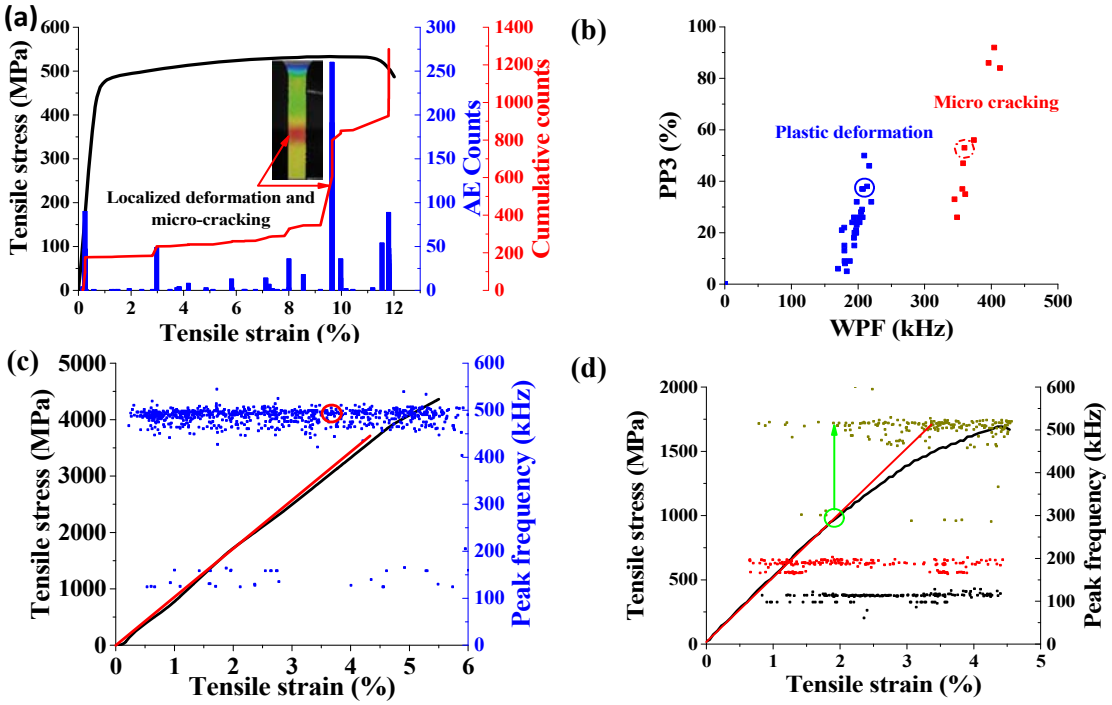

Figure 2. Mechanical behavior and AE response of each constituents of the Glare 1A; (a) Stress-strain curve together with AE data of Al 7475-T761; the red arrow denote changes in AE signature due to localized deformation, (b) AE clustering results on Al 7475 data, (c) stress-strain curve of S2 fiberglass tensile test together with PF AE data, (d) stress-strain curve of prepreg layer together with AE clustering data, green arrow point out the E modulus linearity deflection due to fibers breakage.

3.2. Quasi-static tensile tests of Glare®1A specimens

Figure 3a illustrates a typical stress-strain curve combined with AE amplitudes and PFs obtained by testing Glare®1A with the MTS. The composite was found to exhibit a bilinear mechanical response. The transition from elastic to plastic behavior is found to be sharp compared to the more gradual transition in the alloy (Figure 2a). In addition, there was no localized strain in the composite similar to what was reported for the aluminum testing in Figure 2a. In addition, the range of PFs in the recorded AE activity was found to be between 100-500 kHz and the associated amplitudes ranged from 35-85 dBae. The amplitude of the AE events was found to increase near the transition point and further intensified as the stress approached the failure point. Figure 3b shows the corresponding AE data in

terms of cumulative counts; the AE activity appears to follow an exponential form. In addition, it can be seen that the majority of the AE activity is manifested beyond the elastic-plastic transition. Figure 3c-d illustrate major fracture modes found in post mortem which confirmed the activation of fiber breakage, fiber/matrix interface cracking, matrix cracking and delamination in the metal/matrix-fibers layers.

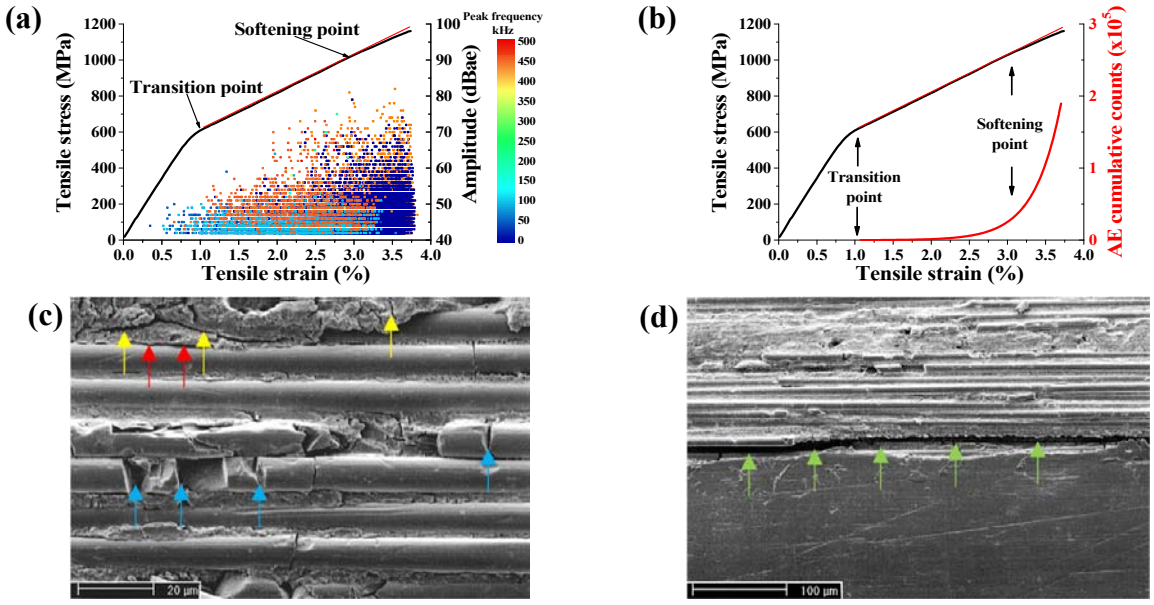

Figure 3. Stress-strain curve of Glare®1A at the lab scale alone along with AE data: (a) in terms of amplitude and PFs, (b) represented by cumulative counts; Post-mortem SEM image showing (c) fibers breakage (blue arrows), fiber-matrix separation (red arrows) and matrix cracking (yellow arrows), (d) Metal-prepreg layer delamination (green arrow)

3.3 In-situ SEM tensile test and AE response of Glare®1A

Figure 3a illustrates the stress-strain curve together with AE data analyzed into clusters by LVQ and expressed by WPF. The mechanical response was found to different from the original one due to the precursory localized narrowing zone. The latter causes to localized strain resulted in parabolic form instead of almost bi-linear behavior for the full specimen. The young's modulus found to be 67 GPa as compare to the calculated 65 GPa and the yield point decreases to 510 MPa as compare to 636 MPa for the full one. The plastic regime shows a considerable strain hardening resulted in fracture stress of 1180 MPa as compare to 1280 MPa for the full test. As for the AE data, three dominant WPFs were detected with three additional mechanisms characterized by low intensity. Similar to the test of full specimen, the AE activity initiated after 0.5%, with damage manifested by matrix cracking (WPF 110 kHz) and plastic deformation of the Al-alloy (WPF 180 kHz) followed by fibers breakage (WPF 400 kHz). The additional WPFs which lie between 180-400 kHz may be related to three minor damage mechanisms, cracking of the interface metal/matrix layers (WPF 200 kHz), microcracking of fiber/matrix interface (WPF 270 kHz), and micro-cracking of the large particles in the Al-alloy (WPF 350 kHz). As shown, the intensity of the fibers breakage increases with the loading while the other two damage mechanisms remain almost constant. The partition to clusters is also displayed in terms of PP3 vs. WPF (Figure 4b), and three dominated damage mechanisms are well observed.

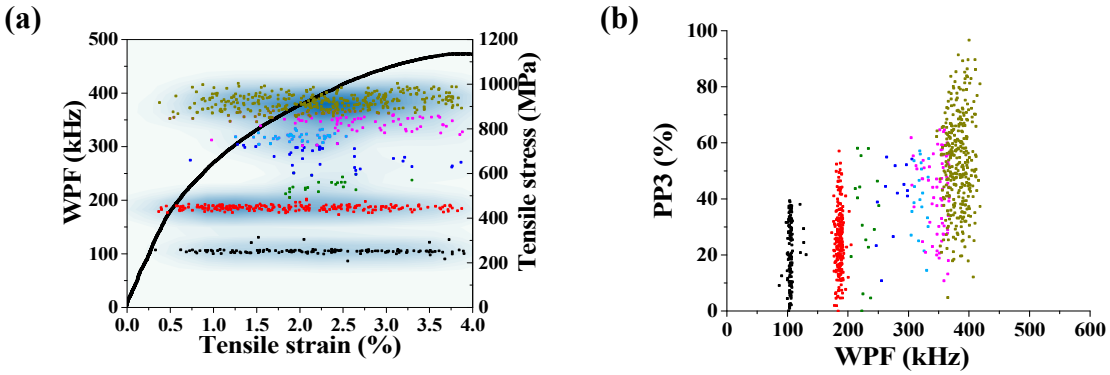

Figure 4. (a) Stress-strain curve of the in-situ SEM miniature specimen together with WPF clusters (colored with density function), (b) The major clusters in terms of PP3 vs. WPF.

High resolution images were taken during the in-situ SEM tensile test simultaneously with AE activity. Figure 5a-c illustrates a general view of the virgin state, at applied strain of 1% and the final fracture respectively, which clearly shows the damage mechanism at the outer surface in terms of fiber breakage and the increase in the cracking density as a function of the applied loading. By selecting AE signals at different stages of loading and performing wavelet analysis, both waveform and frequency characteristics were evaluated and compared to the component results reported earlier. Hence, Al deformation in Figure 6a, matrix cracking, (Figure 6b), fiber breakage (Figure 6c) and a combination of fiber breakage with some indication of interface cracking (Figure 6d).

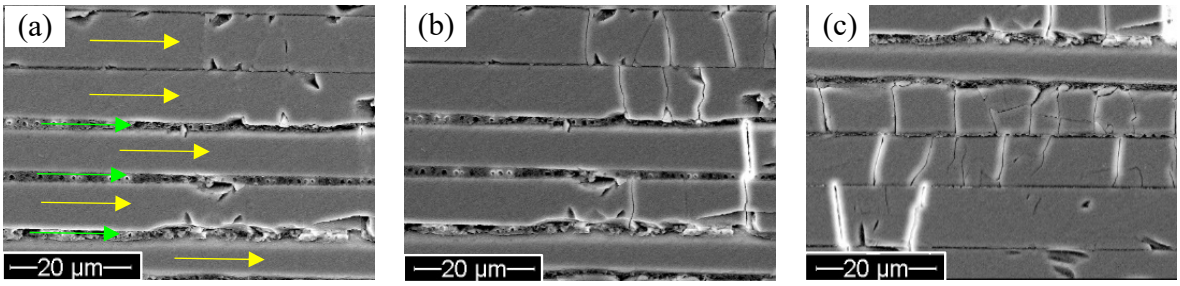

Figure 5. Damage Evolution of the in-situ SEM specimen at (a) virgin state (yellow arrows = S2 fiberglass, green arrows = Epoxy resin), (b) strain level of 1%, (c) strain level of 3%.

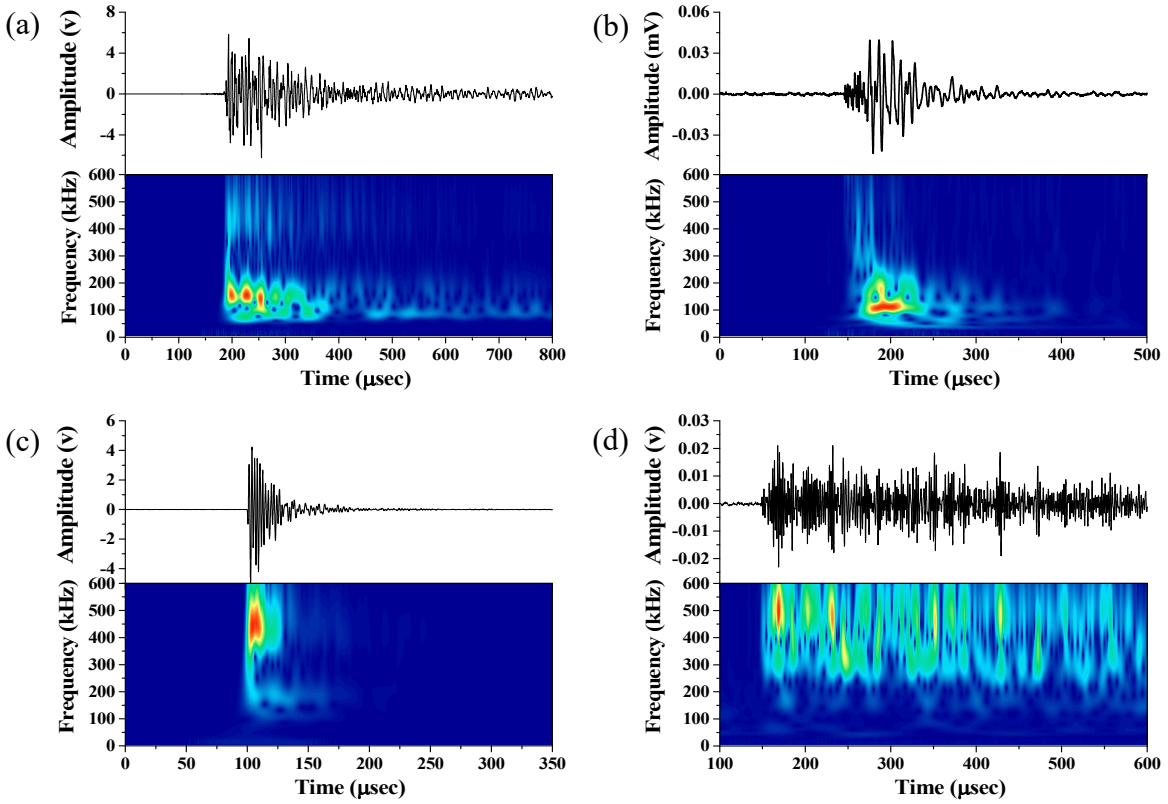

Figure 6. Wavelet analysis of AE signals taken at different stage of loading from the in-situ SEM specimen indication the different damage mechanisms; (a) plastic deformation, (b) Matrix cracking, (c) Fiber breakage, (d) Bundle of fibers breakage with interface cracking

4. Discussion

The mechanical response of Glare®1A is characterized by a bilinear behavior as can be seen in Figure ***3***a. It has a secondary modulus (E_p) at the plastic regime as compared to the higher one at the elastic region. Yielding of the Al layers results in stress transfer from the metal to the fibers layers resulted in fiber breakage together with matrix and interface cracking, which are the main causes to the appearance of E_p. The actual low value of the secondary modulus with linear behavior can be attributed to the competition of two main damage mechanisms. The first one is related to plasticity of the Al alloy layer which contributes to strain hardening while the second one involves fiber breakages resulted in a "softening process". With regard to the AE analysis, fibers start to brake at the transition point, the deviation from linearity can be observed later on due to minor necking phenomena of the Al-layers with accompanied by massive fiber breakage. Talreja suggested a micro mechanical model which describes the damage accumulation in composites as multiple transverse ply cracking (or matrix cracking) [37]. The model with its assumptions can be described by mainly two constraint categories as High constraint and full constraint as illustrated in Figure 7a.

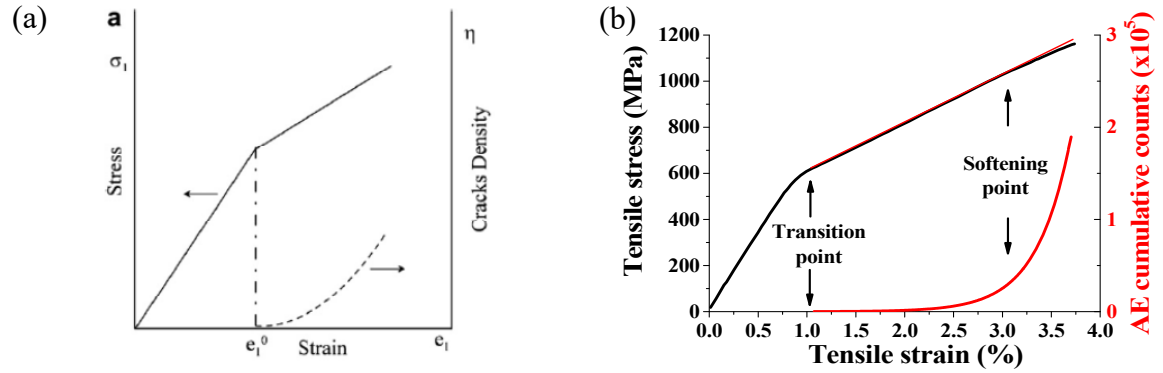

Figure 7. a) bilinear stress–strain behavior for lab scale test with high constraints to transverse cracking associated to transverse crack density [31], b) stress-strain curve with AE cumulative counts - current study

In the current research the exponential profile of the damage model in terms of AE data (Figure 7b) was found to be very similar to the micromechanical damage model suggested by Talreja [38], for inter-laminar cracking in composite laminates such as the tested FRML. Talreja proposed the use of a damage tensor defined as:

$$D_{ij} = \frac{k \cdot t_c^2}{s \cdot t \cdot cos\theta} n_i \cdot n_j \quad (1)$$

Where t is the thickness of the specimen, t_c is the ply thickness, s the crack spacing, θ the angle between the fiber direction and the transverse direction and n = (cosh, sinh, 0). By using a thermodynamic framework for the description of the material response, Talreja further determined a damage model for a bilinear stress–strain curve. This model predicts the crack density based on an exponential function of strain, as shown schematically in Figure 7a by the dashed curve [19]. The predicted profile is in agreement with experimental results such as the ones obtained by Kistner et al. [39]. Similarly, the quasi-static results obtained in this paper are in good agreement with the results obtained by Talreja and Kistner [23].

5. Conclusions

The following conclusions can be drawn from the current study;

1. The bilinear mechanical behavior of Glare®1A in a quasi-static tensile test is a consequence of the competition of several damage mechanisms, including plastic deformation and micro-cracking coalescence due to the presence of hard particles at the Al-Alloy, as well as fibers breakage and interfacial de-bonding at metal/resin layer in addition to fiber/matrix and matrix cracking. As the balance in these mechanisms is interrupted softening process occurs results in deviation from linearity.
2. Based on AE analysis and clustering algorithm, the damage accumulation during quasi-static tensile test of Glare®1A is composed of five main mechanisms which includes matrix cracking, Al yielding, layers delamination, fiber pullout, fiber matrix interface debonding, deformed Al and fibers breakage.
3. The AE data in terms of cumulative counts follows the same trend as suggested by a micro-mechanical model.
4. The proposed NDT&E method was shown to have the capability of tracking damage initiation and its evolution in this composite material.

References

[1] Vlot A, Gunnink JW. *Fibre metal laminates: an introduction*. London: Kluwer Academic Publisher; 2001.

[2] Vlot A, Vogelesang L, De Vries T. Towards application of fibre metal laminates in large aircraft. *Aircraft Engineering and Aerospace Technology*. 1999;71(6):558-570.

[3] Wu G, Yang JM. The mechanical behavior of GLARE laminates for aircraft structures. *JOM*. 2005;57(1):72-79.

[4] Bussiba A, Kupiec M, Ifergane S, Piat R, Böhlke T. Damage evolution and fracture events sequence in various composites by acoustic emission technique. *Composites Science and Technology*. 2008;68(5):1144-1155.

[5] Wu X, Guo Y. Fatigue behaviour and life prediction of fibre reinforced metal laminates under constant and variable amplitude loading. *Fatigue & Fracture of Engineering Materials & Structures*. 2002;25(5):417-432.

[6] Miller RK, McIntire P. *Nondestructive Testing Handbook. Vol. 6: Acoustic Emission Testing*2005.

[7] Hellier C. *Handbook of nondestructive evaluation*. 2nd ed: Mcgraw Hill Press; 2003.

[8] Anastassopoulos A, Philippidis T. Clustering methodology for the evaluation of acoustic emission from composites. *Journal of acoustic emission*. 1995;13(1-2):11-22.

[9] Suzuki H, Kinjo T, Hayashi Y, Takemoto M, Ono K, Hayashi Y. Wavelet transform of acoustic emission signals. *Journal of acoustic emission*. 1996;14(2):69-84.

[10] Hamstad M, O'gallagher A, Gary J. A wavelet transform applied to acoustic emission. *Journal of Acoustic Emission*. 2002;20:39-61.

[11] Pan B, Qian K, Xie H, Asundi A. Two-dimensional digital image correlation for in-plane displacement and strain measurement: a review. *Measurement science and technology*. 2009;20(6):062001.

[12] Cofaru C, Philips W, Van Paepegem W. A novel speckle pattern—adaptive digital image correlation approach with robust strain calculation. *Optics and Lasers in Engineering*. 2012;50(2):187-198.

[13] Hild F, Roux S. Digital image correlation: from displacement measurement to identification of elastic properties–a review. *Strain*. 2006;42(2):69-80.

[14] Pan B. Recent progress in digital image correlation. *Experimental Mechanics*. 2011;51(7):1223-1235.

[15] Schwartz E, Saralaya R, Cuadra J, Hazeli K, Vanniamparambil PA, Carmi R, et al. The use of digital image correlation for non-destructive and multi-scale damage quantification. *SPIE Smart Structures and Materials+ Nondestructive Evaluation and Health Monitoring*: International Society for Optics and Photonics; 2013. p. 86922H-86922H-86915.

[16] Cuadra J, Vanniamparambil PA, Hazeli K, Bartoli I, Kontsos A. Damage Quantification in Polymer Composites using a Hybrid NDT Approach. *Composites Science and Technology*. 2013;83:11-21.

[17] Carmi R, Vanniamparambil P, Cuadra J, Hazeli K, Rajaram S, Guclu U, et al. Acoustic Emission and Digital Image Correlation as Complementary Techniques for Laboratory and Field Research. *Advances in Acoustic Emission Technology*: Springer; 2015. p. 605-622.

[18] Vanniamparambil PA, Bolhassani M, Carmi R, Khan F, Bartoli I, Moon FL, et al. A data fusion approach for progressive damage quantification in reinforced concrete masonry walls. *Smart Materials and Structures*. 2014;23(1):015007.

[19] Talreja R. Continuum modeling of the development of intralaminar cracking in composite laminates. *ICF7*, Houston (USA) 1989, 1989.

[20] Garrett K, Bailey J. Multiple transverse fracture in 90 cross-ply laminates of a glass fibre-reinforced polyester. J*ournal of materials science*. 1977;12(1):157-168.

[21] Laws N, Dvorak G. The loss of stiffness of cracked laminates. *Fundamentals of deformation and fracture*. 1985:119-127.

[22] Hashin Z. Analysis of cracked laminates: a variational approach. *Mechanics of materials*. 1985;4(2):121-136.

[23] Zhang J, Herrmann K. Stiffness degradation induced by multilayer intralaminar cracking in composite laminates. *Composites Part A*: Applied Science and Manufacturing. 1999;30(5):683-706.

[24] McCartney L. Theory of stress transfer in a 0°—90°—0° cross-ply laminate containing a parallel array of transverse cracks. J*ournal of the Mechanics and Physics of Solids*. 1992;40(1):27-68.

[25] Li S. On the unit cell for micromechanical analysis of fibre-reinforced composites. Proceedings of the Royal Society of London A: *Mathematical, Physical and Engineering Sciences*, vol. 455: The Royal Society; 1999. p. 815-838.

[26] Talreja R. A continuum mechanics characterization of damage in composite materials. Proceedings of the Royal Society of London A: M*athematical, Physical and Engineering Sciences*, vol. 399: The Royal Society; 1985. p. 195-216.

[27] Talreja R. Multi-scale modeling in damage mechanics of composite materials. *Journal of materials science*. 2006;41(20):6800-6812.

[28] Talreja R. A synergistic damage mechanics approach to durability of composite material systems. *Progress in durability analysis of composite systems*. 1996:117-129.

[29] Singh CV. A higher order synergistic damage model for prediction of stiffness changes due to ply cracking in composite laminates. *CMC: Computers, Materials & Continua*. 2013;34(3):227-249.

[30] Duan X, Yao W. Multi-directional stiffness degradation induced by matrix cracking in composite laminates. *International journal of fatigue*. 2002;24(2):119-125.

[31] Gudmundson P, Östlund S. First order analysis of stiffness reduction due to matrix cracking. *Journal of composite materials*. 1992;26(7):1009-1030.

[32] Talreja R. Damage characterization by internal variables. *Composite materials series*. 1994:53-53.

[33] Kaminski M, Laurin F, Maire J, Rakotoarisoa C, Hémon E. Fatigue damage modeling of composite structures: the onera viewpoint. *AerospaceLab*. 2015(9):p. 1-12.

[34] Alderliesten RC. Fatigue crack propagation and delamination growth in Glare: *DUP Science*; 2005.

[35] Sause MGR, Gribov A, Unwin AR, Horn S. Pattern recognition approach to identify natural clusters of acoustic emission signals. *Pattern Recognition Letters*. 2012;33(1):17-23.

[36] Sause MG. *In situ monitoring of fiber-reinforced composites: theory, basic concepts, methods, and applications*: Springer; 2016.

[37] Talreja R. Damage analysis for structural integrity and durability of composite materials. *Fatigue & Fracture of Engineering Materials & Structures*. 2006;29(7):481-506.

[38] Talreja R. Damage development in composites: mechanisms and modelling. *The Journal of strain analysis for engineering design*. 1989;24(4):215-222.

[39] Kistner MD, Whitney JM, Browning CE. First-ply failure of graphite/epoxy laminates. *Recent Advances in Composites in the United States and Japan*, ASTM STP. 1985;864:44-61.